World Academy of Science, Engineering and Technology
International Journal of Mechanical and Mechatronics Engineering
Vol:17, No:3, 2023

Evaluating the Validity of Computational Fluid Dynamics Model of Dispersion in a Complex Urban Geometry Using Two Sets of Experimental Measurements

Mohammad R. Kavian Nezhad, Carlos F. Lange, Brian A. Fleck

***Abstract*—**This research presents the validation study of a computational fluid dynamics (CFD) model developed to simulate the scalar dispersion emitted from rooftop sources around the buildings at the University of Alberta North Campus. The ANSYS CFX code was used to perform the numerical simulation of the wind regime and pollutant dispersion by solving the 3D steady Reynolds-averaged Navier-Stokes (RANS) equations on a building-scale high-resolution grid. The validation study was performed in two steps. First, the CFD model performance in 24 cases (eight wind directions and three wind speeds) was evaluated by comparing the predicted flow fields with the available data from the previous measurement campaign designed at the North Campus, using the standard deviation method (SDM), while the estimated results of the numerical model showed maximum average percent errors of approximately 53% and 37% for wind incidents from the North and Northwest, respectively. Good agreement with the measurements was observed for the other six directions, with an average error of less than 30%. In the second step, the reliability of the implemented turbulence model, numerical algorithm, modeling techniques, and the grid generation scheme was further evaluated using the Mock Urban Setting Test (MUST) dispersion dataset. Different statistical measures, including the fractional bias (FB), the mean geometric bias (MG), and the normalized mean square error (NMSE), were used to assess the accuracy of the predicted dispersion field. Our CFD results are in very good agreement with the field measurements.

***Keywords*—**CFD, plume dispersion, complex urban geometry, validation study, wind flow.

I. Introduction

THE urban population in recent decades has shown a drastic rise around the world, and statistical studies have strongly suggested that roughly 70% of the earth's population will be living in urban environments by the next few decades [1]. This urbanization has made controlling the possible health hazards of living in a compact urban area, such as the detrimental effects on air quality, a topic that requires urgent attention. One of the most common sources of air pollution in compact urban settings is the exhaust gas emitting from rooftop stacks. It can significantly affect the quality of fresh air at intakes of the emitting and even surrounding buildings, potentially compromising the well-being of their occupants. To prevent hazards of this kind, we need a clear understanding of how these contaminants are dispersed in different meteorological conditions and in the presence of structural obstacles with varying shapes and dimensions. The constantly varying nature of the meteorological conditions and the complex effects of the airflow interaction with the buildings and structures make predicting the flow pattern extremely challenging.

Full-scale field tests can be performed to understand realistic atmospheric conditions around bluff bodies such as buildings. Effects such as varying inflow patterns, buoyancy forces, atmospheric stratification must be understood to eliminate the problems of poor indoor air quality (IAQ) and sick buildings [2], [3]. However, the varying meteorological conditions, limited number of measurement points, and costs of field studies make it almost impossible to understand all parameters influencing dispersion patterns. Wind tunnel and water channel tests, on the other hand, have the advantage of maintaining controlled and steady test conditions. However, besides missing realistic environmental effects, this method has several disadvantages, including the associated high cost and complicated scaling and similarity issues [4]. The apparent limitations of the full-scale and reduced-scale tests have encouraged many researchers to develop and modify analytical and semi-empirical dispersion models [5]-[7]. These widely used dispersion models were mainly developed relying on optimistic generalizations of the meteorological conditions. They typically simplify the geometrical topographies that lead to poor predictions near the source and in complex terrains where the turbulent flow parameters play an undeniable role in pollutant dispersion.

CFD modeling has proven to be the ideal choice, as it can predict the pollutant concentration and other flow characteristics on a fine grid in the computational domain. Progress has been made to perfect the numerical simulation of the plume dispersion in generalized cases (e.g., isolated buildings, the street canyon between two buildings, flat terrain, etc.) and to assess the effects of different influencing parameters [8]-[10]. However, the prediction of plume dispersion in a complex urban setting is significantly more challenging, due to the behavior of the turbulent flows with large scale recirculation structures and three-dimensional strain

M. R. Kavian Nezhad, C. F. Lange, and B. A. Fleck are with the University of Alberta, Edmonton, Alberta, Canada (phone: +1-780-2218779; e-mail: kavianne@ualberta.ca).

fields which challenge turbulence models. Very few studies have attempted to numerically model and simulate the dispersion within complex urban settings. Often the detailed features of the building layouts are simplified and modeled as simple rectilinear blocks [11], [12]. The lack of details in the CAD models of buildings and their arrangements can often introduce uncertainty to calculations of high-strain regions on the buildings and their surroundings [13]. To address the gap in the field, a detailed CFD model of the University of Alberta North Campus has been created to assess and investigate the wind flow and plume dispersion around the buildings.

Considering that validation of the numerical simulations is an essential part of computer modeling, data from the experimental measurement campaign conducted previously at the north campus [14] were used to validate the flow field generated by this CFD model for eight different wind directions. To further evaluate the capability of this CFD model in predicting the dispersion of the emitting plumes from stacks, the experimental array of the MUST [15] was recreated to examine the reliability of the implemented turbulence model and numerical algorithm.

II. Fundamentals and Mathematical Model

In general, the dynamic of any type of fluid flow can be governed by the following three laws of conservation of mass, conservation of momentum, and the conservation of energy. For this research, the analyzed fluid flow is assumed to be isothermal. The validity of this assumption was verified by calculating the bulk Richardson number (Ri_b) using available meteorological measurements at the considered geometry. The bulk Richardson number, defined by (1), measures the ratio of the buoyancy production to shear production, in which values of $\ll 1$ indicate dominantly mechanically shear-driven flows where the buoyancy effects are negligible.

$$Ri_b = \frac{g\Delta\theta_v \Delta z}{T_v[\Delta u^2 + \Delta v^2]} \tag{1}$$

where g is the gravitational acceleration ($9.81\mathrm{m/s^2}$), $\Delta\theta_v$ is the virtual potential temperature difference, Δz is the height difference at the two selected points, Δu and Δv are the differences between two horizontal components of the velocity at the desired points. The virtual potential temperature in (1) can be expressed by $\theta_v = \theta(1 + 0.609)q$, where $\theta = T(P_0/P)^{0.286}$, q is the specific humidity, P is the air pressure, T is the air temperature, and P_0 is the reference pressure (100 kPa).

Due to the unavailability of the measurements at different vertical levels, Ri_b in two marginal cases of maximum shear gradient (measurements taken at two points located in campus) and maximum temperature gradient (measurements taken at campus and Edmonton International Airport) were calculated as − 0.0119 and 0.0617, respectively. Table I summarizes the measurements used to calculate the Ri_b. Therefore, the energy equation was not used in the context of this research. It should also be noted that the remaining governing equations can be simplified by considering the applicable assumptions, such as steady-state, incompressible airflow, negligible terrestrial Coriolis effect (high Rossby number), constant and isotropic viscosity, and a passive scalar pollutant. The Rossby number (Ro) is defined as the ratio of the inertial forces to the Coriolis forces and can be calculated using $Ro = U/Lf$, where U is the characteristic horizontal velocity, L is the characteristic horizontal length scale, and f is the Coriolis frequency [16]. Considering that the order of magnitudes of these parameters in this research are $U\sim1$, $L\sim10^2$, and $f\sim10^{-5}$, the resulted Ro would be in the order of 10^3 which justifies the assumption of negligible Coriolis effects.

TABLE I
Measurements Used for Calculating the Ri_b

Location	z (m)	T (°C)	P (kPa)	q (g/kg)	u (m/s)	v (m/s)
Campus P.1	64	29.7	100.7	4.46	2.31	−1.07
Campus P.2	68	29.2	100.7	4.33	2.45	0.73
Edmonton International Airport	78	29.7	92.4	5.92	−4.1	0.72

The airflow and pollutant dispersion in the atmospheric boundary layer (ABL) are turbulent, necessitating a closure approach if all time and length scales cannot be resolved. Two widely used methods are Large Eddy Simulation (LES) and RANS. Though LES is believed to produce more realistic unsteady results than RANS, it imposes significantly greater computational demands, making it more suitable for modeling the sudden accidental or deliberate release of hazardous airborne scalars where instantaneous local concentrations are of great importance [17]. Therefore, considering the large size of the computational domain and the interest in the mean quantities of the flow, the RANS method has been chosen to solve the governing equations in this research. Using Reynolds decomposition, the mass and momentum conservation equations can be expressed in their time-averaged forms of (2) and (3), respectively:

$$\frac{\partial \bar{u}_i}{\partial x_j} = 0 \tag{2}$$

$$\bar{u}_j \frac{\partial \bar{u}_i}{\partial x_j} = -\frac{1}{\rho}\frac{\partial \bar{p}}{\partial x_i} + \nu \frac{\partial^2 \bar{u}_i}{\partial x_j^2} - \frac{\partial \overline{u_i' u_j'}}{\partial x_j} \tag{3}$$

where $\bar{u}_i$ is the time-averaged fluid velocity in the three (i, j, k) Cartesian directions, x_i denotes these directions, ρ is the fluid density, and p is the pressure. Supplementary equations are required to close the system of equations represented by (2) and (3), and the available turbulence models can provide that. The Menter Shear Stress Transport (SST) $k-\omega$ turbulence model has been chosen in this research as it is considered to be a hybrid turbulence model by providing a transformation from the $k-\varepsilon$ into $k-\omega$ model near the walls, and using the standard $k-\varepsilon$ model in the fully turbulent regions of the geometry far from the wall [18]. SST $k-\omega$ provides the transport equations for the turbulence kinetic energy per unit mass (k) and the specific dissipation rate (ω) to close this problem:

$$\frac{\partial(\rho k)}{\partial t}+\frac{\partial(\rho k u_i)}{\partial x_i}=\frac{\partial}{\partial x_i}\left[\left(\mu+\frac{\mu_t}{\sigma_k}\right)\frac{\partial k}{\partial x_j}\right]+P_k-\beta^*\rho k\omega \quad (4)$$

$$\frac{\partial(\rho\omega)}{\partial t}+\frac{\partial(\rho\omega u_i)}{\partial x_i}=\frac{\partial}{\partial x_i}\left[\left(\mu+\frac{\mu_t}{\sigma_{\omega,1}}\right)\frac{\partial\omega}{\partial x_j}\right]+\gamma_2\left(2\rho S_{ij}\cdot S_{ij}-\frac{2}{3}\rho\omega\frac{\partial\bar{u}_i}{\partial x_j}\delta_{ij}\right)-\beta_2\rho\omega^2+(1-F_1)\frac{2\rho}{\sigma_{\omega,2}}\frac{\partial k}{\partial x_k}\frac{\partial\omega}{\partial x_k} \quad (5)$$

in which, $S_{ij}=\frac{1}{2}\left(\frac{\partial\bar{u}_i}{\partial x_j}+\frac{\partial\bar{u}_j}{\partial x_i}\right)$, F_1 is the blending factor that guarantees a smooth transition from $k-\omega$ to $k-\varepsilon$ far from the walls, μ_t is the eddy viscosity, $\mu_t=\rho k/\omega$, P_k is the rate of production of turbulent kinetic energy presented by (6), and the remaining model constants have empirical values of $\sigma_k=1.0$, $\sigma_{\omega,1}=2.0$, $\sigma_{\omega,2}=1.17$, $\gamma_2=0.44$, $\beta^*=0.09$, and $\beta_2=0.083$ [19].

$$P_k=\left(2\mu_t S_{ij}\cdot S_{ij}-\frac{2}{3}\rho k\frac{\partial\bar{u}_i}{\partial x_j}\delta_{ij}\right) \quad (6)$$

With the flow field and the turbulent characteristics solved, the concentration of the passive scalar can be calculated separately afterwards by solving (7):

$$u_j\frac{\partial C}{\partial x_j}=D_t\frac{\partial^2 C}{\partial x_j\partial x_j} \quad (7)$$

where C is the mean concentration of the scalar, D_t is the turbulent mass diffusivity expressed by μ_t/Sc_t, and Sc_t is the turbulent Schmidt number. Numerous studies have reported the profound importance of the Sc_t on the turbulent diffusion, which drastically affects the predicted concentration [8]. For the purpose of this research, a widely used value of 0.9 has been considered for Sc_t.

III. CFD Models and Validation of Study Results

CFD has proven to be a powerful and effective tool in predicting the dispersion pattern of a pollutant in complex turbulent flow fields. However, due to the highly complex nature of the turbulent flow, making a series of simplifications and assumptions in every step of modeling is inevitable. Therefore, careful validation of the CFD models with high-quality experimental measurements is necessary to assess the effect of the introduced simplifications. The common practice for validating the dispersion models is to use reliable measurements of tracer gases. Due to the high cost and complexity of tracer experiments in urban regions, acquiring a reliable dispersion dataset in every geometry with unique domain topography and diverse structural arrangement is not feasible. In this regard, the validation study in this research was performed in two steps. First, the CFD models of the North campus for eight different wind directions and three dominant wind speeds were evaluated by comparing the predicted flow fields with the available dataset of the previous measurement campaign by our research group [14]. Furthermore, in the second step, the accuracy of the numerical predictions was investigated using the comprehensive dataset of the MUST experiment to evaluate the reliability of the implemented numerical algorithm and the mathematical model in resolving the dispersion field. The main features of the generated CFD models and results of the validations studies for the mentioned steps are discussed in the following subsections.

A. Validation of the Flow Field

A detailed description of the measurement setup, evaluation method, and the validation results of the wind flow field in the campus geometry for 12 cases (four main wind directions and three wind speeds) is provided in [14]. Hence, a brief overview of the CFD model, extended results, and discussion will be given in the following.

The ANSYS CFX commercial code was used for this research to prepare the numerical models of the wind flow over the University of Alberta campus. This model contains 22 North Campus buildings with varying sizes and shapes that are relatively close to each other, each with unique rooftop structures. A hybrid finite-element/finite volume approach was used to discretize the Navier-Stokes equations. Hexahedral elements were used to mesh parts of the computational domain where no buildings are present, while tetrahedral elements were considered for regions around the buildings. Extra refinements were performed near all the walls, roofs, and ground to capture boundary layer gradients, accurately generating numerous prismatic layers (Fig. 1). The height of the tallest building in the geometry ($H_{max}\approx 65$ m) was considered to determine the size of the computational domain following the COST guidelines for ABL modeling [20]. Using this, a distance of $5H_{max}$ was set between the building complex and the inlet, the lateral sides, and the top of the computational domain, while a distance of $15H_{max}$ from the last building and the outlet was specified.

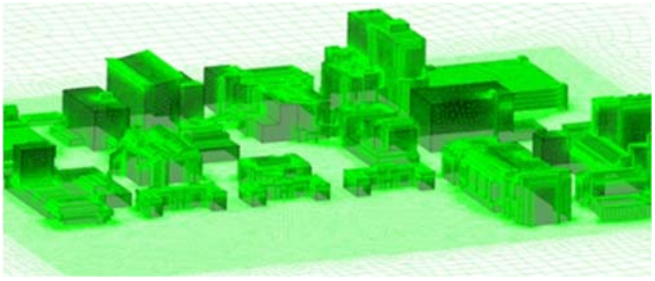

Fig. 1 Generated computational grid for campus geometry [14]

Accurate prediction of the flow field in an ABL simulation strongly depends on the appropriate definition of the boundary conditions. The inlet wind flow and turbulence profiles have the most profound effects among all the boundaries. They account for the impact of the upstream terrain roughness (not included in the computational domain) and the available vertical wind gradient in the ABL. A comprehensive review conducted by Blecken et al. suggests that many studies have considered the equilibrium boundary layer in the ABL by assuming a constant vertical shear [21]. Following this common practice, our work uses the mean logarithmic velocity profile (U) and the turbulence quantities profiles (k and ε) derived by Richards and Hoxey [22] at the inlet of the computational domain. Considering the SST $k-\omega$ turbulence model used in this

study, the dissipation rate ε is converted to the specific dissipation rate, ω, by (11):

$$U = \frac{u_\tau}{\kappa} ln\left(\frac{z+z_0}{z_0}\right) \quad (8)$$

$$k = \frac{u_\tau^2}{\sqrt{C_\mu}} \quad (9)$$

$$\varepsilon = \frac{u_\tau^3}{\kappa(z+z_0)} \quad (10)$$

$$\omega = \varepsilon / C_\mu k \quad (11)$$

where u_τ is the friction velocity associated with the logarithmic wind speed profile, z is the vertical displacement, and z_0 is the aerodynamic roughness length, κ is the von Karman constant with a value of 0.412, and C_μ is a model constant (0.09). An aerodynamic roughness length of 1 m was considered, assuming the terrain in this study with several buildings of various heights [23]. The reference wind speed at a height of 64 m was estimated using the measurements collected from the weather station on the roof of the University of Alberta's Henry Marshall Tory Building (the tallest building in the vicinity) [14]. Furthermore, the outlet plane of the computational domain is considered to have zero relative pressure, while the top and side planes were set to symmetry. All the solid surfaces on the geometry (building walls, roofs, and grounds) were set to no-slip walls. As discussed previously, SST $k-\omega$ resolves the boundary layer near the walls by using the low Reynolds formulations. Therefore, the ANSYS CFX automatic near-wall treatment method was applied to smoothly switch between wall functions and low-Reynolds number grids. Three different grid resolutions were analyzed, and the normalized velocity profiles along a vertical line above the roof, near the west edge of the tallest building, were assessed. Eventually, the grid with 8,309,837 nodes was selected as it showed a better resolution of the turbulent boundary layer compared to the coarse grid (5,530,761 nodes) while providing nearly identical results to the fine grid (11,020,616 nodes) [14].

Measurements from three anemometers installed on the roof of the tallest building of the campus (Donadeo ICE) provided a sample view of the wind flow field. The hourly averaged measurements of the reference wind speeds and directions obtained from the weather station on the Tory building roof were processed to create individual directional bins that only contained wind directions in the range of $\theta \pm 5°$. The dataset was further filtered, and measurements were sorted by wind speed for each reference wind speed with the permitted range of $U_{ref} \pm 5\%$. Simulations were run for three dominant wind speeds (4, 5, and 6 m/s) and eight directions, and results were evaluated using the SDM presented at [14]. Table II provides the average percent error of the deviations between numerical and experimental speeds for the eight incident wind directions.

The results of Table II indicate that the wind incidents of North and Northwest show the most significant calculated deviations. In comparison, a relatively good agreement is observed between the CFD results and the measurements for all other six directions, with an average percent error of generally less than 30%. One possible reason of the relatively larger deviations calculated for the North and Northwest wind incidents is that upstream computational domain in these cases does not include the available geographical landscapes (e.g., the deep valley and the river). The North Saskatchewan River runs in a valley adjacent to the North and West side of the Donadeo ICE building, positioned to the Northwest of the computational domain. For this reason, the inflow wind speed and turbulence profiles estimated by (8)-(11) are not ideally representative of the actual inlet boundary condition. Various thermally induced fluctuations are also generated in the turbulent flow upstream of the domain with the interaction of the air with the ground and river water and solar irradiance that could affect the realism of the numerical predictions. Therefore, modifications in inflow profiles for the North and Northwest incidents would be helpful to understand the effects of the upstream geography. In the end, based on the presented validation study and calculated deviations between numerical results and measurements, the CFD models of the wind flow around the campus geometry are deemed as acceptable, bearing in mind the uncertainties associated with estimates of the North and Northwest wind incidents.

TABLE II
AVERAGE PERCENT ERROR OF NUMERICAL SPEEDS FOR EACH INCIDENT WIND DIRECTION

	North	North East	East	South East	South	South West	West	North West
Free Stream Speed 4 m/s								
Error in Velocity (%)	48.80	24.32	19.97	17.88	19.89	21.08	27.46	35.40
Free Stream Speed 5 m/s								
Error in Velocity (%)	52.11	26.43	5.56	13.73	17.12	24.41	21.39	32.81
Free Stream Speed 6 m/s								
Error in Velocity (%)	52.76	29.12	6.87	15.21	16.06	25.72	25.06	37.48

B. Validation of the Dispersion

In addition to evaluating the predicted flow field by the CFD model, the reliability of the implemented equations, numerical scheme, and modeling techniques was tested to solve the scalar transport equation and estimate the pollutant concentration field. The pollutant is assumed as a passive scalar, meaning that due to its low mass fraction in the field and its non-reactive nature, its concentration has no effect on the conservation of momentum or bulk continuity. Therefore, the transport equation was solved only after the flow field was estimated. Consequently, having the validated model of the dispersion flow coupled with the already validated flow field model, a

fully validated CFD model is achieved to simulate dispersion around the campus buildings.

The MUST dataset was chosen in this research as it provides high-quality and comprehensive measurements of the series of tracer gas experiments [24]-[28]. The MUST experiment was designed in a simulated urban geometry, with the primary purpose of providing a valuable dataset that includes the meteorological and dispersion data for validating and verifying the accuracy of the dispersion models and CFD simulations. In their experimental setup, a 10 by 12 array of shipping containers were placed in the center of the test domain over relatively flat ground. The containers were 12.2 m long, 2.4 m wide, and 2.5 m high, forming an approximately 200 m × 200 m square array. This valuable dataset contains comprehensive and high-quality measurements of 68 dispersion trials: 63 with continuous releases and five with puff releases. Propylene was used as the tracer, with 37 different source locations at various horizontal and vertical locations, within and upstream of the array, which provided a rich collection of case studies.

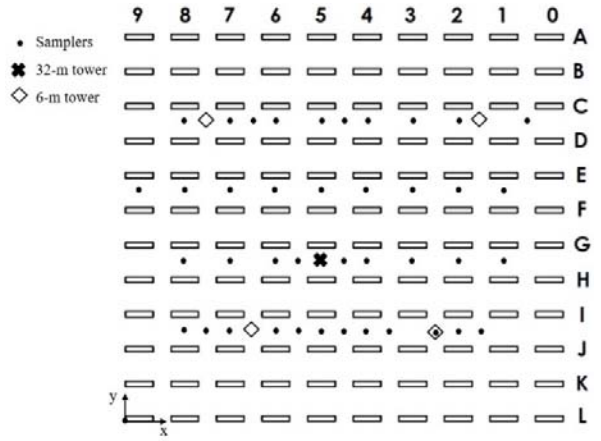

Fig. 2 Planar schematic view of MUST container array. Rectangles correspond to shipping containers

Sampling and concentration measurements were collected using 48 Digital Photoionization Detectors (dPID) and 24 Ultra Violet Ion Collectors (UVIC) to accommodate measurements at different horizontal and vertical locations. The horizontal concentration field was mapped using 40 dPIDs located in four parallel lines downstream of the source at the height of 1.6 m above the ground. The horizontal sampling lines are numbered as 1 to 4, with line 1 located between rows I and J and line 4 between rows C and D (Fig. 2). Eight dPIDs on the 32-m central tower and 6 UVIC on each of the four 6 m towers located in every quadrant of the array were used to measure the concentrations at different vertical levels. In an attempt to collect data in neutral and stable atmospheric conditions, trials were done mainly in the early mornings or nights and 15 minutes periods [15].

A careful assessment of all the 68 trials is necessary to select suitable case studies for CFD model validation. The selected case studies should contain high-quality measurements and represent diverse yet roughly analogous test conditions to the expected cases of dispersion flow at campus geometry.

One of the primary purposes of developing the detailed model of campus geometry was to accurately predict the dispersion pattern of the pollutants around the buildings and near the fresh air intakes. Taking the continuous emissions from these stacks into account, the test cases with puff releases of the tracer gas in the MUST array were out of scope for our research. Further review of the measurement data narrowed the possible cases to 36 trials, in which the detected tracer gas on the central tower and most of the horizontally distributed samplers showed substantial concentrations. Furthermore, the trials conducted in neutral or stable atmospheric conditions were filtered by referring to the calculated mean Obukhov length (L_O) of each trial [29]. The Obukhov length (L_O) has shown to be a practical scale in determining the level of atmospheric stability as it shows the height where the turbulence generated by buoyancy is stronger than that caused by wind shear [24]. Considering the assumption of the neutral atmospheric conditions in the isothermal CFD model of dispersion around campus, only trials with Obukhov lengths ranging from 130 m to 28000 m were used for validation study. Table III summarizes the final four selected trials with all the necessary quantities (mean values of the 200 seconds quasi-steady period calculated by Yee and Biltoft [29]) required for accurately modeling the dispersion flow. The quantities included in Table III are the tracer release rate (q_s), source height (Z_s), the upstream wind speed at 4 m height (S_{04}), the upstream wind direction at 4 m height (α_{04}), friction velocity at 4 m height on the central tower (u^τ), Obukhov length at 4 m height on the central tower (L_O), and the turbulence kinetic energy at 4 m height on the central tower.

TABLE III
SELECTED FOUR TRIALS OF MUST FIELD EXPERIMENT FOR THE VALIDATION STUDY

Trial No.	Trial name	$q_s\ \left(\frac{l}{\min}\right)$	Z_s (m)	$S_{04}\ \left(\frac{\mathrm{m}}{\mathrm{s}}\right)$	α_{04} (deg)	u^τ (m/s)	L_O (m)	k (m^2/s^2)
1	2681829	225	1.8	7.93	−41	1.10	28000	1.46
2	2672213	200	1.8	2.68	30	0.35	150	0.428
3	2682320	225	2.6	4.55	−39	0.50	170	0.718
4	2692250	225	1.3	3.38	36	0.37	130	0.537

Similar to the procedure for modeling the wind flow around the campus geometry, the dispersion flow throughout the MUST array was modeled using ANSYS CFX code. Considering the size of the MUST array and maximum height of the obstacles within $H = 2.5$ m, a nested computational domain with an inner domain of $230\ \mathrm{m} \times 210\ \mathrm{m} \times 20\ \mathrm{m}$ and outer domain of $470\ \mathrm{m} \times 450\ \mathrm{m} \times 80\ \mathrm{m}$ was defined. The parts of the domain with no available structures were meshed using hexahedral elements, and unstructured tetrahedral elements were considered to mesh the inner domain. The inflow

wind speed and turbulence profiles were estimated using (8)-(11) at the inlet boundaries. The reference wind speeds measured at the reference height of 4 m upstream of the MUST array were used along with the aerodynamic ground roughness of 0.045 m [15].

The dependency of the CFD results on the grid size was examined with three different grid resolutions of 6,387,224 nodes (coarse), 9,909,189 nodes (medium), and 13,963,368 nodes (fine). Figs. 3 and 4 exhibit the predicted concentration profiles at the horizontal sampling line 1 and vertical central mast by the three mentioned grids, respectively. It is obvious that there are minimal deviations between the predicted concentration fields by the medium and fine grids, which justifies the use of the medium grid throughout this research.

The performance of the CFD model in accurately predicting the plume concentration field was evaluated. In this regard, the CFD results are assessed using the statistical method introduced by Chang and Hanna [30] that includes a series of statistical measures extensively used to assess the validity of numerical models, by comparing with field grade measurements.

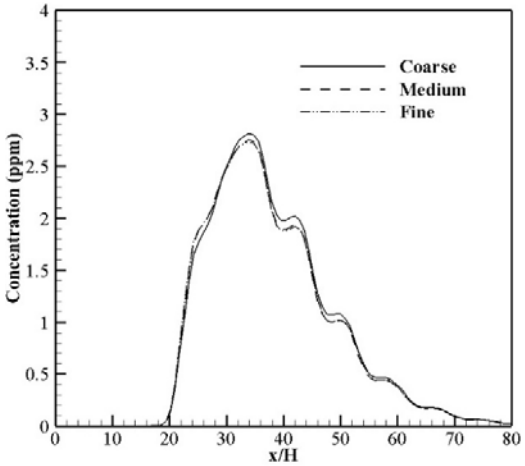

Fig. 3 Comparison of concentration profiles at the first horizontal sampling line in Trial 2681829

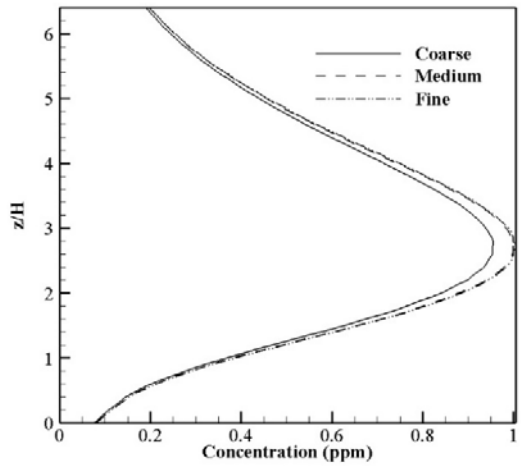

Fig. 4 Comparison of concentration profiles at the central mast in Trial 2681829

The performance measures that will be calculated in this research are FB, MG, NMSE, the geometric variance (VG), and the fraction of numerical data that falls within a factor of two of the field measurements ($0.5 < C_p/C_o < 2$). It should be noted that in cases of dispersion modeling where the concentration varies significantly from point to point, calculating all the mentioned statistical parameters is highly suggested, to capture both the linear systematic bias (FB and NMSE) and the random scatter of the data changing on different orders of magnitude (MG and VG). These performance measures for dispersion modeling are defined as follows, where C_o is the observed concentration, C_p is the predicted concentration by the CFD model, and $\bar{C}$ is the average concentration value over the entire dataset:

$$FB = \frac{(\overline{C_o} - \overline{C_p})}{0.5(\overline{C_o} + \overline{C_p})} \tag{12}$$

$$MG = \exp\left(\overline{\ln C_o} - \overline{\ln C_p}\right) \tag{13}$$

$$NMSE = \frac{\overline{(C_o - C_p)^2}}{\overline{C_o}\,\overline{C_p}} \tag{14}$$

$$VG = \exp\left[\overline{\left(\ln C_O - \ln C_p\right)^2}\right] \tag{15}$$

The ideally accurate CFD model would generate results that give FB and NMSE of 0, and MG, VG, and FAC2 of 1. In practice, Chang and Hanna [30] suggested acceptable ranges for these performance measures by investigating several dispersion datasets that are $-0.3 < FB < 0.3$, $NMSE < 4$, $VG < 1.6$, $0.7 < MG < 1.3$, and $FAC2 > 0.5$. However, extra considerations are required when calculating the logarithmic measures as they are significantly sensitive to the small values and return undefined values for zero concentrations. Therefore, as suggested by Chang and Hanna [30], a threshold equal to the sampler's detection precision (0.04 ppm in case of the MUST dataset) is used for the averaged concentrations when MG and VG are calculated.

Table IV presents the calculated statistical measures for the point-to-point comparison in all the four selected trials. As it can be concluded, the calculated FB has values within the acceptable range in all four cases, with predicted data showing slight over-prediction in Trial 2 and Trial 3 (negative values) and minor under-prediction of concentration field in Trial 1 and Trial 4. Taking all the measured concentration data of the four trials, the CFD model shows a minimal overall over-prediction (FB = −0.05). The MG, the ratio of geometric average observed concentration to geometric average predicted concentration, is shown to be in the recommended range for all the cases, with an overall value of 1.01 for all the data. The calculated NMSE was also shown to be within the acceptable range for all the trials, with an overall value of 1.50.

It should be noted that the relatively large NMSE of Trial 3 (3.55) corresponds to the oddly large deviations between the predicted and observed concentration at only two sampling points, which when removed can reduce the NMSE of this trial to 0.633. The VG represents the unsystematic scatter of the

predictions and is calculated to be larger than the acceptable limit for all cases. That refers to a relatively large scatter that is mainly due to the available deviations at the edge of the plume, where the concentrations are relatively low, and even slight differences between observed and predicted values could lead to considerably large VG values. The CFD model was capable of predicting 66% of all the measurements within a factor of 2 of the observed values, which justifies the validity of this model.

TABLE IV
STATISTICAL EVALUATION OF THE CFD MODEL FOR THE FOUR SELECTED TRIALS OF THE MUST DATASET

Statistical quantities	Trial 1	Trial 2	Trial 3	Trial 4	All
FAC2	0.62	0.74	0.62	0.65	0.66
FB	0.04	−0.12	−0.09	0.11	−0.05
NMSE	0.79	0.91	3.55	0.55	1.50
VG	3.11	2.96	3.31	1.85	2.56
MG	1.23	1.15	1.21	0.98	1.01

To further assess the accuracy of the CFD model, the predicted horizontal and vertical data were also evaluated; the calculated statistical measures are presented in Table V. As the statistical quantities suggest, the model performs better in predicting the concentration field of the scalar on vertical lines with 81% of the values within the factor of 2 of the observed concentrations. Additionally, less scatter is observed in vertical lines (VG = 2.09) than all horizontal sampling lines. The negative values of FB for all vertical and the two first horizontal lines (sampling lines of 1 and 2) indicate an overall over-prediction. In contrast, the opposite is observed for the two farther horizontal sampling lines where the model generally under-predicts. The under-prediction of the scalar concentration on sampling line 4 is observed to be much higher than the other lines, with the calculated FB that being higher than the recommended value (FB = 0.73). Consequently, larger scatter (VG = 5.08 and NMSE = 2.21) is observed on this line and only 53% of the predicted concentrations are within the factor of 2 of the observed values.

TABLE V
STATISTICAL EVALUATION OF THE CFD MODEL BASED ON THE GEOMETRIC LOCATIONS OF THE ASSIGNED SENSORS

Statistical quantities	Line 1	Line 2	Line 3	Line 4	Vertical
FAC2	0.65	0.58	0.64	0.53	0.81
FB	−0.22	−0.06	0.27	0.73	−0.12
NMSE	1.27	0.72	1.09	2.21	1.23
VG	2.59	3.30	3.80	5.08	2.09
MG	0.82	0.97	1.02	1.67	1.03

To better evaluate the overall performance of the CFD model in predicting the scalar concentration field, scatter diagrams are presented for the horizontal (Fig. 5) and vertical (Fig. 6) sampling lines. Overall, good agreement between the predicted and measured concentrations can be observed for both the horizontal and vertical sampling lines with approximately 60% and 81% of the predictions within the factor of 2, respectively. The predicted concentrations with relatively high values that belong to the samplers near the source (e.g., sampling line 1) and along the plume centerline, are shown to be closer to the 1:1 line, while the predicted lower concentrations, mostly far from the source and the plume centerline, show considerably more scatter. Constantly varying meteorological conditions during field measurements could be the source of these relatively higher scatters. In this regard, the effects of the inlet boundary conditions on the accuracy of the predicted results were investigated by examining the wind direction in Trial 2. As mentioned, the provided quantities in Table III are, in fact, the calculated mean values over the 200 second quasi-steady period, which could be a source of deviation between numerical results and measurements. Considering the standard deviation of 7.9˚ in the instantaneous inflow wind direction in Trial 2 [29], two more cases were simulated with different inflow wind directions of 22.1˚ and 37.9˚. Fig. 7 shows the substantial deviation in the predicted concentration field caused by minor variations in the inflow wind direction during the field measurements, which further emphasizes the presence of discrepancies that could not be avoided.

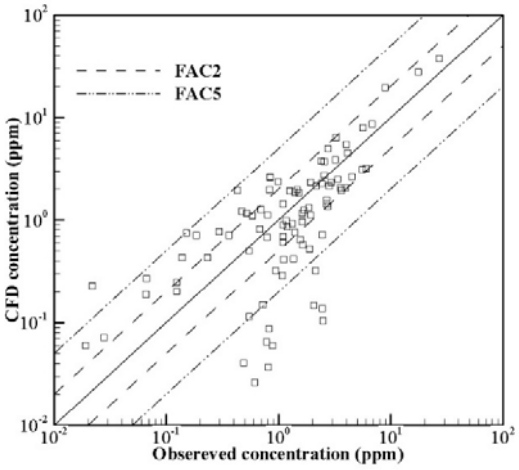

Fig. 5 Scatter diagrams between the predicted and observed concentrations in horizontal sampling lines for all the trials

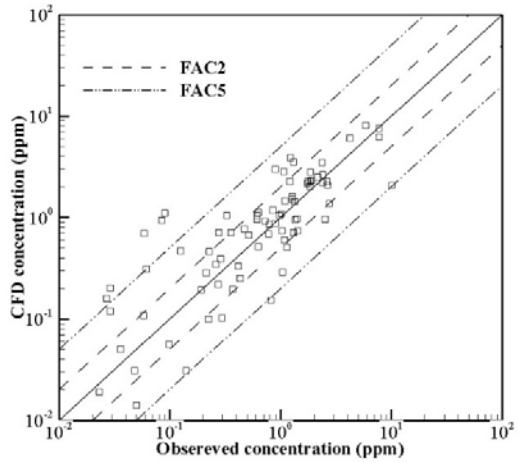

Fig. 6 Scatter diagrams between the predicted and observed concentrations on vertical sampling lines for all the trials

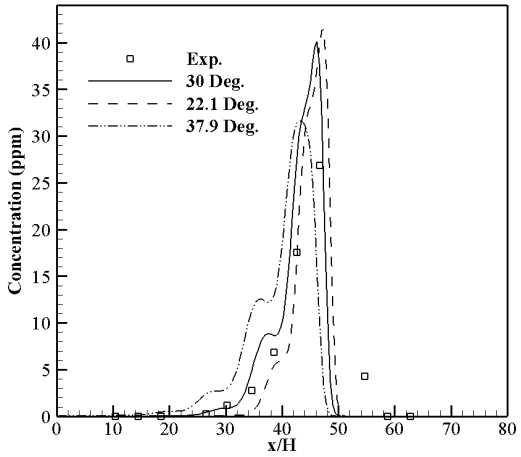

Fig. 7 Comparison of concentration profiles at the first horizontal sampling line in trial 2672213 for different inflow wind directions

IV. Conclusion

A two-step validation study was carried out to assess the accuracy of an atmospheric dispersion CFD model in a complex urban setting, in which the tracer experiment dataset was not available at the studied geometry.

First, the capability of the model to accurately predict the flow field within the University of Alberta North Campus was evaluated by comparing the numerical results with wind speeds and directions of a previously conducted measurement campaign at the campus geometry.

The second step assessed the reliability of the implemented modeling methods, turbulence model, transport equation, and the numerical scheme, by reconstructing the dispersion trials of the MUST experiment.

The predicted results in both steps showed good agreement with the observed quantities. Since the tracer gas (or the pollutant in future studies) is assumed to be a passive scalar due to its non-reactive nature and low mass fraction, its associated interference to the fluid motion in the domain is negligible. As a result, the transport equation can be solved after the flow field has been resolved in geometry, justifying the proposed validation approach in this study. Further investigation is necessary to assess the uncertainties associated with this validation approach by conducting parametric studies and making cross-comparisons in both geometries.

References

[1] 2018 revision of world urbanization prospects. Tech. rep., United Nations Department of Economic and Social Affairs (UNDESA), 2018.

[2] H. L. Higson, R. F. Griffiths "Concentration measurements around an isolated building: A comparison between wind tunnel and field data", Atmospheric Environment, Vol. 28, No. 11, pp. 1827-1836, 1994.

[3] S. Oikawa, Y. Meng, "A field study of diffusion around a model cube in a suburban area", Boundary-Layer Meteorology, Vol. 84, pp. 399-410, 1997.

[4] M. Lateb, R. N. Meroney, M. Yataghene, H. Fellouah, F. Saleh, M. C. Boufadel "On the use of numerical modeling for near-field pollutant dispersion in urban environment", Environmental Pollution, Vol. 208, pp. 271-283, 2016.

[5] ASHRAE, "Building air intake and exhaust design", ASHRAE Fundamental Handbook, American Society of Heating, Refrigerating and Air-conditioning Engineers, Atlanta, United States, 2011.

[6] N. S. Holmes, L. Morawska, "A review of dispersion modeling and its application to the dispersion of particles: an overview of different dispersion models available", Atmospheric Environment, Vol. 40, pp. 5902-5928, 2006.

[7] ADMS 3 user guide, Cambridge Environmental Research Consultants Limited, Cambridge, UK, 2004.

[8] Tominaga, Y., Stathopoulos, T., "CFD simulation of near-field pollutant dispersion in the urban environment: A review of current modeling techniques", Atmospheric Environment. Vol. 79, pp. 716-730, 2013.

[9] X. Huang, L. Gao, D. Guo, R. Yao, "Impacts of high-rise building on urban airflows and pollutant dispersion under different temperature stratifications: Numerical investigations", Atmospheric Pollutant Research, Vol. 12, pp. 100-112, 2021.

[10] E. Keshavarzian, R. Jin, K. Dong, K. C. S. Kwok, Y. Zhang, M. Zhao, "Effect of pollutant source location on air pollutant dispersion around a high-rise building", Applied Mathematical Modeling, Vol. 81, pp. 582-602, 2020.

[11] Y. Du, B. Blocken, S. Abbasi, S. Pirker, "Efficient and high-resolution simulation of pollutant dispersion in complex urban environments by island-based recurrence CFD", Environmental Modelling and Software, Vol. 145, 2021.

[12] F. T. Silva, N. C. Reis, J. M. Santos, E. V. Goulart, C. E. Alvarez, "The impact of urban block typology on pollutant dispersion" Journal of Wind Engineering and Industrial Aerodynamics, Vol. 210, 2021.

[13] A. Ricci, I. Kalkman, B. Blocken, M. Burlando, A. Freda, and M. Repetto, "Local-scale forcing effects on wind flows in an urban environment: Impact of geometrical simplifications" Journal of Wind Engineering and Industrial Aerodynamics, Vol. 170, pp. 238-255, 2017.

[14] S.J. Mattar, M. R. Kavian Nezhad, M. Versteege, C. F. Lange, B. A. Fleck, "Validation Process for Rooftop Wind Regime CFD Model in Complex Urban Environment Using an Experimental Measurement Campaign", Energies, 2021.

[15] C.A. Biltoft, "Customer Report for Mock Urban Setting Test", Technical report, DPG Document No. WDTC-FR-01–121. US Army Dugway Proving Ground, Dugway, Utah, 2001.

[16] A. Speranza, V. Lucarini, "Environmental science, physical principles and applications", Encyclopedia of Condensed Matter Physics, pp. 146-156, 2005.

[17] X. Zheng, H. Montazeri, B. Blocken, "CFD simulations of wind flow and mean surface pressure for buildings with balconies: Comparison of RANS and LES" Building and Environment, Vol. 173, 2020.

[18] H. K.Versteeg, W. Malalasekera, "Introduction to Computational Fluid Dynamics", Second Edi., vol. M. 2012.

[19] F. R. Menter, "Two-Equation Eddy-Viscosity Turbulence Models for Engineering Applications", AIAA Journal, Vol. 32, No. 8, pp. 1598-1605, 1994.

[20] J. Franke, A. Hellsten, H. Schlünzen, and B. Carissimo, "Guideline for the CFD Simulation of Flows in the Urban Environment: COST Action 732 Quality Assurance and Improvement of Microscale Meteorological", no. May. 2007.

[21] B. Blocken, T. Stathopoulos, J. Carmeliet, "CFD simulation of the atmospheric boundary layer: wall function problems" Atmospheric Environment, Vol. 41, pp. 238-252, 2007.

[22] P. J. Richards and R. P. Hoxey, "Appropriate boundary conditions for computational wind engineering models using the k-ε turbulence model," J. Wind Eng. Ind. Aerodyn., vol. 46–47, no. C, pp. 145–153, 1993.

[23] WMO Guide to Meteorological Instruments and Methods of Observation WMO-No. 8 page I.5-13.

[24] M. Milliez · B. Carissimo "Numerical simulations of pollutant dispersion in an idealized urban area, for different meteorological conditions", Boundary Layer Meteorology. 122 (3), pp. 321-342, 2007.

[25] R.P. Donnelly, T.J. Lyons, T. Flassak, "Evaluation of results of a numerical simulation of dispersion in an idealised urban area for emergency response modelling", Atmospheric Environment. Vol. 43, pp. 4416-4423, 2009.

[26] P. Kumar, A. Feiz, S. K. Singh, P. Ngae, "An urban scale inverse modelling for retrieving unknown elevated emissions with building-resolving simulations", Atmospheric Environment. Vol. 140, pp. 135-146, 2016.

[27] M. L. Bahlali, E. Dupont, B. Carissimo "Atmospheric dispersion using a Lagrangian stochastic approach: Application to an idealized urban area under neutral and stable meteorological conditions", Journal of Wind Engineering and Industrial Aerodynamics, Vol. 193, 2019.

[28] C. Teea, E.Y.K. Nga, G. Xub, "Analysis of transport methodologies for pollutant dispersion modelling in urban environments", Journal of

Environmental Chemical Engineering, Vol. 8, 2020.
[29] Yee, E., Biltoft, C., "Concentration fluctuation measurements in a plume dispersing through a regular array of obstacles", Boundary Layer Meteorology. 111 (3), pp. 363-415, 2004.
[30] J. C. Chang, S. R. Hanna, "Air quality model performance evaluation", Meteorological Atmospheric Physics, 87 (1-3), pp. 167-196, 2004.